Ocean Systems Engineering, *Vol. 8, No. 4 (2018) 381-407*
DOI: https:// doi.org/10.12989/ose.2018.8.4.381

A zonal hybrid approach coupling FNPT with OpenFOAM for modelling wave-structure interactions with action of current

Qian Li[1], Jinghua Wang[1], Shiqiang Yan[*1], Jiaye Gong[2] and Qingwei Ma[1]

[1]School of Mathematics, Computer Science and Engineering, City, University of London Northampton square, London, EC1V 0HB, UK
[2]College Of Shipbuilding Engineering, Harbin Engineering University, Nangang District, Harbin, Heilongjiang Province, 150001, China

(Received July 17, 2018, Revised September 4, 2018, Accepted September 17, 2018)

Abstract. This paper presents a hybrid numerical approach, which combines a two-phase Navier-Stokes model (NS) and the fully nonlinear potential theory (FNPT), for modelling wave-structure interaction. The former governs the computational domain near the structure, where the viscous and turbulent effects are significant, and is solved by OpenFOAM/InterDyMFoam which utilising the finite volume method (FVM) with a Volume of Fluid (VOF) for the phase identification. The latter covers the rest of the domain, where the fluid may be considered as incompressible, inviscid and irrotational, and solved by using the Quasi Arbitrary Lagrangian-Eulerian finite element method (QALE-FEM). These two models are weakly coupled using a zonal (spatially hierarchical) approach. Considering the inconsistence of the solutions at the boundaries between two different sub-domains governed by two fundamentally different models, a relaxation (transitional) zone is introduced, where the velocity, pressure and surface elevations are taken as the weighted summation of the solutions by two models. In order to tackle the challenges associated and maximise the computational efficiency, further developments of the QALE-FEM have been made. These include the derivation of an arbitrary Lagrangian-Eulerian FNPT and application of a robust gradient calculation scheme for estimating the velocity. The present hybrid model is applied to the numerical simulation of a fixed horizontal cylinder subjected to a unidirectional wave with or without following current. The convergence property, the optimisation of the relaxation zone, the accuracy and the computational efficiency are discussed. Although the idea of the weakly coupling using the zonal approach is not new, the present hybrid model is the first one to couple the QALE-FEM with OpenFOAM solver and/or to be applied to numerical simulate the wave-structure interaction with presence of current.

Keywords: hybrid model; wave-current-structure interaction; FNPT; NS solver; QALE-FEM; OpenFOAM

1. Introduction

Wave-structure interaction has been a research focus on offshore, coastal and ocean engineering for many years. For safety and survivability of the structures, extreme wave condition must be considered. In various scenarios, the current effects need to be incorporated. Both experimental

*Corresponding author, Reader, E-mail: shiqiang.yan@city.ac.uk

http://www.techno-press.org/?journal=ose&subpage=7 ISSN: 2093-6702 (Print), 2093-677X (Online)

and numerical studies have been carried out aiming to explore (1) the current effects on the wave diffraction from the structure (Ning *et al.* 2014, Feng and Bai 2016); (2) the free surface effects on the vortex shedding resulting from flow around submerged structures (Liang 2014, Ozdil and Akilli 2015, Reichl *et al.* 2005, Bai *et al*. 2016, Bai *et al*. 2017) ; or (3) hydrodynamic forces on and flow pattern near the structures subjected to the combination of the wave and current (Isaacson and Cheung 1993, Chaplin and Subbiah 1997, Hu *et al*. 2016, Xiao *et al*. 2013, Kim *et al*. 2016, Chung 2016, Li and Lin 2010). Readers may be referred to Bai *et al.* (2017) and other papers indicated above for a detailed review.

The current mainly poses two aspects of effects on the wave-structure interaction problems. The first one is that the presence of current may significantly modify the characteristics of ocean waves (e.g., Wang 2018, Yan *et al*. 2010, Wu and Yao 2004, Ryu *et al*. 2003, Kharif *et al*. 2009, Lavrenov and Porubov 2006). The second one is the current-structure interaction with presences of the free surface, typically featured by the flow separation and vortex shedding (e.g., Stringer *et al*. 2014). For the first aspect, accurately modelling extreme wave with current effects usually requires a large-scale (~10s km) and long-duration (e.g., 3-hour sea state) numerical simulation to capture the spatial-temporal propagation of the ocean wave (Wang *et al*. 2016, 2018). For this purpose, various numerical models have been developed based on the shallow water equations (e.g., Chen *et al*. 2005), the fully nonlinear potential theory (FNPT) solved by using the boundary element method (Kim and Kim 1997, Kim *et al*. 1998, Büchmann *et al*. 2000, Ferrant 2001, Teng *et al*. 2001, Lin and Li 2003) and finite element method (Yan *et al*. 2010), Fast Fourier Transform based High Order Spectrum method (e.g., Dommermuth and Yue 1987), Spectral Boundary Integral model (e.g., Grue and Jensen 2012) and Enhanced Spectral Boundary Integral model (Wang *et al*. 2018). These models are relatively computationally efficient but fail to resolve the small- to micro-scale physics near the structures, i.e., the feature of the second aspect of the problem indicated above. On the other hand, numerical models based on the multi-phase Navier-Stokes equation (NS) e.g., Bai *et al*. (2016), Bai *et al*. (2017), Xiao *et al*. (2013), Kim *et al*. (2016), Chung (2016), are able to well address the second aspect of the problem and to resolve detailed flow pattern near the structure. However, their high computational demands make them difficult to be applied to large-scale and long-duration simulations in order to capture the evolution of the extreme waves under the action of current. Consequently, in engineering practices, these models are usually applied in a small computational domain near the structures with pre-described inlet wave conditions. Usually, such wave conditions are either specified by simplified wave theories, e.g. linear/2^{nd} order wave theory and NewWave theory (Xiao *et al*. 2013, Kim *et al*. 2016). These initiate the developments of hybrid approaches combining a simplified but more effective model, e.g., the FNPT, and a NS model for robustly modelling the large-scale wave-current field and their interaction with structures.

The fundamental idea of the hybrid approach is that in the regions where the viscous/turbulent effects are significant, e.g., near the breaking waves and the structures (referred to as NS domain), the NS model is utilised to resolve small- and micro-scale physics, e.g., the vortex shedding and flow separation; in other regions, where the viscous/turbulent effects play insignificant role, a simplified model, e.g., assuming the flow is incompressible, inviscid and irrotational, is employed. Two strategies have been adopted to realise the idea. The first one is called velocity-decomposition or functional-decomposition approach (e.g., Ferrant *et al*. 2003, Edmund *et al*. 2013). In this approach, the velocity and pressure resulting from the NS model are split into two parts, one (referred to as non-viscous part) is the solutions of a simplified theory, e.g., the potential theory or the Euler's equation, and the other (called complementary part) is the remaining part, which is

governed by a complementary equation derived from the difference between the NS model and the simplified equations. In the entire computational domain, the simplified equation is solved, yielding the solutions of the non-viscous part; in the NS domain, the complementary equation is solved, leading to the complementary part of the velocity/pressure, assuming their values in other regions are zero. Overall, the velocity and pressure in the entire computational domain satisfying the NS model are obtained using the summation of the non-viscous part and the complementary part. A well-known example is the so-called SWENSE model, which has been used for simulating the wave-structure interactions in many sea-keeping studies (Luquet *et al*. 2007, Ferrant 2008). The second strategy is often referred to as the domain-decomposition, zonal or spatially hierarchical approach (Fujima *et al*. 2002, Luchaume *et al*. 2003, Biausser *et al*. 2004, Colicchio *et al*. 2006, Janssen *et al*. 2010, Narayanaswamy *et al*. 2010, Yan and Ma 2010, Kim *et al*. 2010, Guo *et al*. 2012, Hildebrandt *et al*. 2013, Sriram *et al*. 2014, Fourtakas *et al*. 2017, Yan and Ma 2017, Higuera *et al*. 2018). By using this approach, the NS domain is governed by the NS model and others are governed by the simplified models, e.g. the FNPT; a single interface or an overlap zone exists between two domains; the velocity and pressure are transferred or exchanged from one domain to another. Many hybrid models have been developed using the zonal approach. These may be classified into weak coupling and strong coupling. For the former, the simplified model only provides data for the NS model at specific locations, e.g. the boundary or the relaxation zone of the NS domain and the NS model does not disturb the simulation of the simplified model (Luchaume *et al*. 2003, Biausser *et al*. 2004, Janssen *et al*. 2010, Narayanaswamy *et al*. 2010, Yan and Ma 2010, Hildebrandt *et al*. 2013, Fourtakas *et al*. 2017, Higuera *et al*. 2018). For the latter the NS model also feedbacks data to the simplified model, e.g. providing the boundary condition of the simplified model (Fujima *et al*. 2002, Colicchio *et al*. 2006, Kim *et al*. 2010, Guo *et al*. 2012, Sriram *et al*. 2014, Yan and Ma 2017). A detailed review on the developments of the hybrid models using the zonal approach can be found in Sriram and Ma (2014). Nevertheless, these approaches are mainly developed and applied to the modelling of large-scale extreme waves and/or their interaction with structures without considering the action of the current.

Considering the fact that the fully nonlinear interaction between the extreme wave and the current needs to be taken into account, an appropriate choice of the simplified model is the FNPT, e.g., the Quasi Arbitrary Lagrangian Eulerian Finite Element Method (QALE-FEM) (Sriram and Ma 2014, Fourtakas *et al*. 2017, Yan and Ma 2017). In addition, the presence of the current may lead to additional numerical challenges. One typical challenge is that the current drives a continuous movement of the particle/nodes in the Lagrangian numerical methods for solving the FNPT model and NS model (e.g., Sriram and Ma (2014), Fourtakas *et al*. (2017), Yan and Ma (2017)), yielding an unsatisfactory particle distribution or mesh distortion. This paper presents a hybrid model to combine the QALE-FEM (Wang *et al*. 2018, Ma and Yan 2009, Yan and Ma 2007) with the OpenFOAM/InterDyMFoam solver adopting a two-phase NS model, which is solved by using the finite volume method (FVM) and volume of fluid (VOF) for identifying the phase. A weakly coupling zonal approach is applied to couple two models. OpenFOAM/InterDyMFoam utilises either a fixed Eulerian grid or a dynamic mesh technique based on an arbitrary Lagrangian Eulerian (ALE) description of the NS model. The original QALE-FEM adopts a Lagrangian form of the FNPT, in order to tackle the challenge associated with the presence of the current, the FNPT model in the QALE-FEM is written as a corresponding ALE form. Furthermore, for the purpose of improving the robustness of the hybrid model, an effective gradient estimation and interpolation approach, the quadric semi-analytical finite difference interpolation (QSFDI) (Yan *et al*. 2018), is applied. The present hybrid model is validated by comparing its numerical prediction with the

experimental data or numerical results available in the public domain. Satisfactory agreements have been observed.

2. Mathematical models and numerical approaches

The problem addressed in this paper will be modelled in a numerical wave tank, as illustrated in Fig. 1, where a wavemaker is utilised on the left end of the tank to generate the incoming waves, a self-adaptive wavemaker is mounted on the right end of the tank for wave absorption. A Cartesian coordinate system is used with the *oxy* plane on the mean free surface and with the *z*-axis being positive upwards. The origin of the coordinate system is located at the intersection between the centre of the structure and the mean water surface. Only a uniform horizontal current $\vec{U}_C(U_{cx}, U_{cy}, 0)$ is applied in this paper, considering the fact that the time and length scales of current are much larger than those of the waves (Ning *et al*. 2014, Wang *et al*. 2018). The FNPT model and the NS model will be applied in different area of the wave tank.

2.1 FNPT model and QALE-FEM method

In Ω_{FNPT}, the fluid is assumed to be incompressible, inviscid and irrotational and so the velocity field can be described by the velocity potential. The total velocity potential (Φ) is expressed by $\Phi = \phi + \vec{r} \cdot \vec{U}_C$ where $\vec{r}(x, y, z)$ is the position vector; ϕ is the rest of the velocity potential apart from $\vec{r} \cdot \vec{U}_C$. The total velocity potential satisfies the Laplace's equation $\nabla^2 \Phi = 0$, yielding

$$\nabla^2 \phi = 0 \tag{1}$$

in Ω_{FNPT}. A wavemaker is implemented in the left end of the tank to generate the waves and a self-adaptive wavemaker is adopted in the right end of the tank for wave absorption. On the wavemaker boundaries, Γ_{WM}, the velocity potential satisfies,

$$\frac{\partial \Phi}{\partial n} = \vec{n} \cdot \left(\vec{U} + \vec{U}_C\right) \; or \; \frac{\partial \phi}{\partial n} = \vec{n} \cdot \vec{U} \tag{2}$$

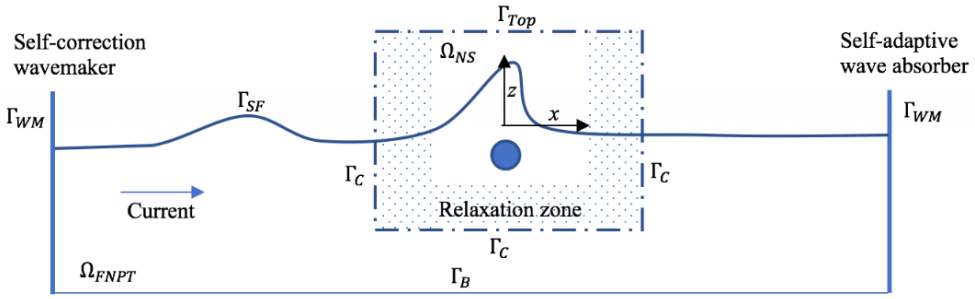

Fig. 1 Sketch of the hybrid model

where $\vec{U}$ and $\vec{n}$ are the velocity and the outward unit normal vector of the rigid boundaries Γ_{WM}, respectively. It can be seen in Eq. (2) that the condition for ϕ on the wavemaker does not depend on the current speed and so the wavemaker generating the waves described by ϕ allows free passage of uniform current. The velocities of the wavemakers in the left and right end of the tank are assigned by using the self-correction wave generation mechanism (Ma *et al*. 2015) and a localised self-adaptive wave absorber (Yan *et al*. 2016), respectively. Since the numerical wavemaker techniques adopted here allows the free passage of the uniform current, the entire numerical wave tank is not closed and the current flux will not be built up in the tank. On the seabed, Γ_B, a slip condition $\partial\phi/\partial n = 0$ is applied.

On the free surface Γ_{SF}, $z = \eta$, where η is the surface elevation, both the kinematic and dynamic boundaries are specified. These conditions can be written in a Lagrangian form (e.g., Ryu *et al*. 2003, Guo *et al*. 2012, Ma *et al*. 2015, Celebi 2001), in which the computational nodes on the free surface move following the motion of the fluid particles

$$\frac{D\vec{r}}{Dt} = \nabla\phi + \vec{U}_C \tag{3a}$$

$$\frac{D\phi}{Dt} = -gz + \frac{1}{2}\left(|\nabla\phi|^2 - \left|\vec{U}_C\right|^2\right) \tag{3b}$$

where D/Dt is the substantial (or total time) derivative following the fluid particles; g is the gravitational acceleration. Using this approach, the normal velocity of the free-surface nodes on the wavemaker, $\vec{n}\cdot(\vec{U}+\vec{U}_C)$ differs from that of the wavemaker, $\vec{n}\cdot\vec{U}$, resulting in that these nodes move away from the wavemaker if the current is non-zero. Due to this, the computational mesh may not fit the wavemaker boundary. To avoid the problem, one may regenerate the mesh (remeshing/ regriding) at every time step as suggested in the BEM proposed by Ryu *et al*. (2003) and Celebi (2001). However, the remeshing/regriding may lead to extra numerical diffusion (Celebi 2001). Alternatively, the free-surface nodes may be moved only vertically, i.e., the horizontal position of free-surface nodes remaining the same. Such approach is referred to as a semi-Lagrangian form (e.g., Huang *et al*. 2007)

$$\frac{\delta\eta}{\delta t} = \frac{\partial\phi}{\partial z} - \left(\nabla\phi + \vec{U}_C\right)\cdot\nabla\eta \tag{4a}$$

$$\frac{\delta\phi}{\delta t} = -\frac{1}{2}|\nabla\phi|^2 - g\eta - \vec{U}_C\cdot\nabla\phi - \frac{1}{2}\left|\vec{U}_C\right|^2 + \frac{\delta\eta}{\delta t}\frac{\partial\phi}{\partial z} \tag{4b}$$

in which $\delta/\delta t$ is the time derivative following the vertical motion of nodes, whose velocity $\vec{v}_m$ is given as (0, 0, $\delta\eta/\delta t$), $\nabla\eta$ stands for the gradient vector of the wave elevation, i.e., ($\frac{\partial\eta}{\partial x}$, $\frac{\partial\eta}{\partial y}$, 0). Clearly, this method is not suitable for the cases involving a moving wavemaker unless an interpolation method is applied. More unfavourably, Eq. (4) is not suitable for dealing with overturning waves, because the gradient of the wave elevation ($\nabla\eta$) may become infinite in these cases. To overcome the difficulties, the free-surface nodes are proposed here to be moved by a scheme which uses the similar principle to an arbitrary Lagragian- Eulerian (ALE) formulation. Specifically, their horizontal velocities v_{mx} and v_{my} in *x*- and *y*-directions, respectively, are taken as

$$v_{mx} = \beta\left(\frac{\partial\phi}{\partial x} + \varepsilon U_{cx}\right), v_{my} = \beta\left(\frac{\partial\phi}{\partial y} + \varepsilon U_{cy}\right) \tag{5a}$$

where ε and β are weighting coefficient and their values range from 0 to 1. To satisfy the kinematic free surface boundary condition ($\eta(x,y,t)$-z =0), the vertical velocity (v_{mz}) of the free surface nodes is taken as

$$\frac{\delta\eta}{dt} = \frac{\partial\phi}{\partial z} - \left(\nabla\phi + \vec{U}_C + \vec{v}_m\right)\cdot\nabla\eta \tag{5b}$$

where $\delta/dt = \partial/\partial t + \vec{v}_m \cdot \nabla$ is the time derivative following the nodal velocity $\vec{v}_m(v_{mx}, v_{my}, v_{mz})$. The corresponding dynamic free surface condition then becomes

$$\frac{\delta\phi}{dt} = -\frac{1}{2}|\nabla\phi|^2 - g\eta - \vec{U}_C\cdot\nabla\phi - \frac{1}{2}\left|\vec{U}_C\right|^2 + \vec{v}_m\cdot\nabla\phi \tag{5c}$$

When ε =1 and $\beta = 1$, Eq. (5) becomes the same as Eq. (3), the Lagrangian form of the free surface conditions; whereas, $\beta = 0$, Eq. (5) is consistent with Eq. (4), the semi-Lagrangian form of the free surface conditions. It should be noted that if ε and β are given any value less than 1, Eq. (5) contains the terms of $\nabla\eta$, which may become infinite when wave overturning is involved as indicated above. Therefore, to deal with the wave overturning, one needs just to assign ε = 1 and $\beta = 1$ where the overturning occurs. Our previous publication (Yan *et al*. 2010) has proposed the ALE form of the free surface conditions with $\beta = 1$. Following Yan *et al*. (2010), the coefficient ε is specified as

$$\varepsilon = \begin{cases} 0 & d_{wm} < L_c \\ \frac{d_{wm} - L_c}{L_c} & L_c \le d_{wm} \le 2L_c \\ 1 & d_{wm} > 2L_c \end{cases} \tag{6}$$

where d_{wm} denotes a horizontal distance between the nodes and the wavemaker and L_c indicates the size of the zone with non-zero ε. Our numerical tests suggest that L_c = min($3d$,$3\lambda_{min}$), in which λ_{min} is the wavelength corresponding to the highest-frequency component of a wave group, is suitable for all cases presented in this paper. In this paper, the ALE form of the boundary conditions is further extended to a more general description with spatially various β. One may adjust the variation of β to optimise the motion of the free surface nodes to maintain a good quality of the computational mesh. For example, when a fixed structure, either submerged or floating, is involved in the computational domain, the nodes on the structure surface is fixed and the movement of the free surface nodes following the Lagrangian way may lead to a significant mesh distortion. More importantly, the variation of β is also expected to bring numerical benefit on the development of the hybrid model, which will be discussed in the following section regarding the coupling. The principle of assigning the value of β is that $\beta = 1$ in the area near the wavemaker, i.e. $d_{wm} \le 2L_c$, and/or in the area where the wave breaking is expected. By using this way, at the wavemaker or in the area near it, the horizontal nodal velocity components are $\partial\phi/\partial x$ and $\partial\phi/\partial y$ in x- and y-directions, respectively. This ensures that the nodes on wavemaker always move to follow with it. In the area where the wave breaking occurs, ε =1 and $\beta = 1$, which allowing the formation of overturning. Thus, the problems related to updating nodes near the wavemaker in the Lagrangian approach and the limitation of the semi-Lagrangian

approach in treating overturning waves are overcome. It is noted that Eqs. (5) become invalid if the wave overturns within the range $d_{wm} < 2L_c$. In such a case, $\varepsilon = 1$ and $\beta = 1$ may be applied with a proper remeshing technique in the area near the wavemaker. It is also worth noting that the mathematical model summarised above is a generalised model on the basis of previous applications, with further extension on introducing varying β. When the current is not involved and $\beta = 1$, the model becomes that used by Yan and Ma (2010), which has capacity of modelling 3D overturning waves with promising accuracy; when the current is involved and $\beta = 1$, it is the same as that adopted by Yan *et al*. (2010) for modelling 2D overturning waves in uniform current.

The problem described above is solved by using a time step marching procedure. At each time step, the boundary value problem (BVP) for the velocity potential is solved by the finite element method (FEM). The details about the FEM formulation have been described in our previous publications (e.g., Ma and Yan 2009, Yan and Ma 2010) and will not be repeated here. The distinguishing feature of the QALE-FEM is that the computational mesh moves to conform to the motion of the free surface and the structures, e.g. the wavemakers, using a purpose-developed spring analogy method. The details of the mesh-moving algorithm can be found in Ma and Yan (2009) and Yan and Ma (2010). In this algorithm, the free surface nodes move following Eqs. (5) in most of the time steps and are re-allocated at a certain frequency to prevent them from becoming too close to or far from others. To re-allocate the free surface nodes, the nodes on the waterline are re-distributed by adopting a principle for a self-adaptive mesh and the others (inner-free-surface nodes) are moved using a spring analogy method. Two methods have been suggested for the inner-free-surface nodes. When wave overturning does not occur, they are first moved in the horizontal plane of the free surface, resulting in new coordinates *x* and *y*; and then the elevations of the free surface corresponding to the new coordinates are evaluated by an interpolating method. When wave overturning occurs, they are first moved in the local tangential plane. After that, a new position of the nodes on the free surface is found by interpolation in the local coordinate system. When reallocating the free surface mesh using the spring analogy method, larger spring stiffness are suggested to the area where a finer mesh resolution is required, e.g., near the wave crest. The effectiveness of the technique has been demonstrated in Yan and Ma (2007) for conserving the mesh quality near the moving structures, e.g., the floating body and wave maker. Additional results are given in Fig. 2, which gives the meshes at two instants for focusing wave groups under strong opposing current, to demonstrate the ability of the mesh-moving technique on ensuring denser mesh near the area with steeper local wave profile.

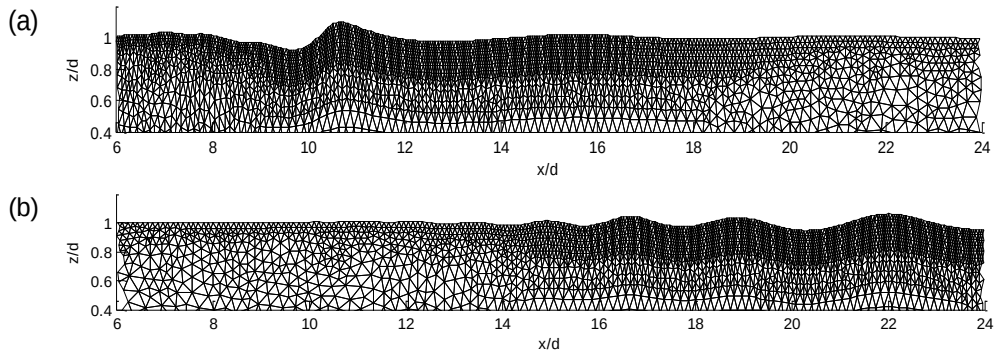

Fig. 2 Mesh near the highest crest recorded at (a) $t = 125\sqrt{d/g}$ and (b) $t = 160\sqrt{d/g}$ (uni-directional focusing wave with opposing current)

As observed, when $t = 125\sqrt{d/g}$ (Fig. 2(a)), the mesh is finer near the highest crest at $x \approx 11d$ and courser at other region such as that near $x \approx 22d$; when the wave group propagates further downstream, e.g. at the moment shown in Fig. 2(b), the highest crest occurs at $x \approx 22d$ and the mesh becomes finer near $x \approx 22d$ and coarser at the position away from the region, e.g., around $x \approx 11d$. This clearly demonstrates that the finer mesh region follows the highest crest.

2.2 Two-phase incompressible NS model

In the NS domain, Ω_{NS}, a two-phase NS model is applied. Both the air and water phases are assumed to be incompressible. The phases and the interface between two phases are identified by the volume of fluid (VOF) method, in which a volume fraction α is defined. The governing equations include the continuity equation, the Reynolds-Averaged Navier-Stokes Equations (RANS) and the transportation equation for the volume fraction

$$\frac{\partial \rho}{\partial t} + \nabla \cdot \rho\vec{u} = 0 \tag{7a}$$

$$\frac{\partial \rho\vec{u}}{\partial t} + \nabla \cdot (\rho\vec{u}\vec{u}) = -\nabla p - \vec{g} \cdot \vec{r}\nabla\rho + \nabla \cdot \left(\mu_{eff}\nabla\vec{u}\right) + \nabla\vec{u} \cdot \nabla\mu_{eff} \tag{7b}$$

$$\frac{\partial \alpha}{\partial t} + \nabla \cdot \alpha\vec{u} + \nabla \cdot \vec{u}_c\alpha(1-\alpha) = 0 \tag{7c}$$

where ρ is the density of the fluid, p the pseudo dynamic pressure, $\vec{u}$ the fluid velocity; μ_{eff} is the effective dynamic viscosity and is the summation of the molecular dynamic viscosity and the turbulent viscosity, which can be determined by using the turbulence modelling, e.g., the well-known $k-\varepsilon$ and $k-\omega$ models. One may find that an artificial compression term $\nabla \cdot \vec{u}_c\alpha(1-\alpha)$ is introduced in Eq. (7(c)), which is only effective in the interfacial zone with $0 < \alpha < 1$. The surface tension is ignored in Eq. (7(b)), considering a large-scale modelling of the ocean waves. Eqs. (7) and corresponding boundary conditions are solved by a finite volume method using open source code OpenFOAM (Jacobsen *et al*. 2011, Higuera *et al*. 2013), which adopts PIMPLE algorithms, merging Pressure Implicit with Splitting of Operators (PISO) and Semi-Implicit Method for Pressure-Linked Equations (SIMPLE), for velocity-pressure coupling. For incompressible two-phase flow, the solver InterDyMFoam is favourable. The details of the governing equation, numerical methods and the OpenFOAM can be found in the above cited paper and relevant online resources.

2.3 Coupling FNPT model with NS model

The main contribution of this paper is to couple the FNPT model, described in Section 2.1 and the NS solver, summarised in Section 2.2 using a zonal approach, as sketched in Fig. 1. As discussed in the Introduction, both weak and strong coupling approaches are available in the literature, although their applications to the problems addressed in this paper are rarely found. For the strong coupling, the solutions to the FNPT model and those to the NS model are sought simultaneously with exact satisfaction of the boundary conditions on the interface, Γ_C, between the FNPT domain and the NS domain. Usually, these conditions are unknown prior to solving both

models and, therefore, an iterative procedure may be required (Sriram *et al*. 2014, Yan and Ma 2017). For the weak coupling, the FNPT model provides the boundary conditions at Γ_C for the NS model, which does not feedback to the FNPT model (Yan and Ma 2010, Hildebrandt *et al*. 2013). This approach does not require iteration. However, when the reflected wave in the NS domain reaches the boundary Γ_C, it will be re-reflected and eventually affect the accuracy of the simulation. One may impose a relaxation zone/damping zone near the boundary to absorb such undesirable reflected waves (e.g., Fourtakas *et al*. (2017)). In this paper, the weak coupling approach with a relaxation zone technique is implemented. In this approach, the FNPT domain (Ω_{FNPT}) covers the entire computational domain without the structure and the QALE-FEM will be used to solve the FNPT model; whereas the NS domain (Ω_{NS}) only covers limited area near the structure (bounded by a dashed line in Fig. 1). In a small area Ω_{NS} attached to the boundary Γ_C, a relaxation zone (shadowed area in Fig. 1) is applied. Due to the fact that the structure is not included in the Ω_{FNPT}, the wave modelled in the numerical wave tank cannot consider the disturbance due to the presence of the structure, i.e. the reflected waves and associated turbulence behaviour. Nevertheless, the FNPT model can provide an accurate solution of the wave-current inlet conditions for the NS model, in which such disturbances are absorbed in the relaxation zone as described below, thus will not be considered in the FNPT model. In the hybrid model, the condition applied at the boundary Γ_C in the NS is the velocity inlet, similar to Jacobsen *et al*. (2011), where the volume fraction and the fluid velocity are specified by using the FNPT solutions. At the boundary Γ_{TOP}, a pressure outlet condition is applied.

Fundamentally, there are two critical issues need to be addressed for a successful coupling of the FNPT and NS models. The first issue is the data exchange between the FNPT domain and the NS domain. As shown in previous sections, the main physical quantities in the FNPT model are the velocity potential ϕ and the surface elevation η; whereas those in the NS model include the velocity $\vec{u}$, pressure p and the volume fraction α. In the present hybrid model, the volume fraction at a surface cell *C*, α_C, on Γ_C are given by the ratio of wetted surface area, A_W, against the total area of the cell, A_C. Detailed numerical formulation may be found in Yan and Ma (2010), Jacobsen *et al*. (2011) and Higuera *et al*. (2013). The velocity $\vec{u}$, pressure p on Γ_C can be found using

$$\vec{u}(x,y,z) = \begin{cases} \nabla\phi(x,y,z) + \vec{U}_c & z \le \eta \\ \nabla\phi(x,y,\eta) + \vec{U}_c & z > \eta \end{cases} \tag{8a}$$

$$p(x,y,z) = \begin{cases} -\rho_w \frac{\partial\phi}{\partial t} - \rho_w \frac{|\vec{\nabla}\phi|^2}{2} - \rho_w g z & z \le \eta \\ 0 & z > \eta \end{cases} \tag{8b}$$

in which ρ_w is the density of the water; the time derivative $\frac{\partial\phi}{\partial t}$ in the FNPT is also obtained by solving a corresponding BVP, as described in (Ma and Yan 2009, Yan and Ma 2007). It is noted that the FNPT is a single-phase model only describing the water flow. In Eq. (8(a)), the velocity of the flow above the free surface (i.e. the air phase) are specified by the corresponding water velocity on the free surface to ensure a smooth transition of the fluid velocity from the water phase to the air phase. The second critical issue to be addressed is how to ensure the continuity/consistence of the solutions on Γ_C and its surrounding area. This problem is mainly caused by two factors. One is that the reflected waves by the structures are considered in the NS model but are ignored in the FNPT model, as discussed above. The second one is due to the fact

that on the boundary Γ_C, the velocity and pressure are imposed by the solution of the FNPT model, in which the flow is assumed to be inviscid/irrotational and the pressure is predicted by the Bernoulli's equation, whereas at other area of the NS domain, the viscosity and the turbulence are taken into account. To address this, a relaxation zone technique is applied. In the relaxation zone, the velocity and the pressure are taken as a weighted summation of the solutions to the NS model and those to the FNPT model

$$f(x,y,z) = f_{NS}(x,y,z)w + f_{FNPT}(x,y,z)(1-w) \tag{9}$$

where *f* is a physical quantity, i.e., the velocity, pressure or the volume fraction; subscripts NS and FNPT denote the solutions to the NS model and the FNPT model, respectively; *w* is the weighting function, which is 0 on the boundary Γ_C and 1 on the inner boundary of the relaxation zone. One may select different weighting functions including exponential, cosine functions (Jacobsen *et al*. 2011, Higuera *et al*. 2013). $f_{FNPT}(x,y,z)$ in Eq. (9) is also obtained by using Eqs. (8). This does not only ensure a smooth transition of the solution from the FNPT model to the NS model, but also effectively absorb the reflected wave and avoid undesirable re-reflection from Γ_C.

As shown, the hybrid model requires the estimation of the velocity using the FNPT solution, i.e. Eqs. (8), for both assigning the boundary condition of the NS solver and implementing the relaxation zone technique. To do so, a gradient calculation by using discretised data (velocity potential at nodes around the specific position $\vec{r}(x,y,z)$) is required to find $\nabla\phi(x,y,z)$ at every time step and considerable numbers of positions inside the relaxation zone. Considering the fact that the computational mesh used by the FNPT is unstructured (see Fig. 2 for demonstration) and moves during the simulation. The finite difference schemes using regularly distributed data points are not suitable. In the present hybrid method, the QSFDI (Yan and Ma 2018), which was recently developed by the authors of this paper, is applied. The consistence and the accuracy of the QSFDI are at the same level as the quadric moving least square method (MLS) or weighted least square method (WLS). But it is expected to demand less computational effort due to the fact that the sizes of the matrices to be inversed in the QSFDI is considerably smaller than the MLS or WLS. Γ_C and the relaxation zone in the NS domain is fixed, and, therefore, the positions $\vec{r}(x,y,z)$, where Eq. (8) and Eq. (9) are applied to obtain $\vec{u}(x,y,z)$ from the FNPT solver, are fixed due to the application of the Eulerian grid in the OpenFOAM/InterDyMFoam for the problem with fixed structures. A key factor of the QSFDI, as well as the MLS and WLS, for accurately estimating the gradient is the determination of the nodes within the support domain of $\vec{r}(x,y,z)$. In the QALE-FEM, they are specified by using the mesh connectivity, e.g., two-three layers of the nodes surrounding the node closest to $\vec{r}(x,y,z)$ depending on the mesh resolutions. To locate the closest node for a specific position, a sub-group of nodes in the QALE-FEM may be pre-specified for each position $\vec{r}(x,y,z)$, so that one only needs to compare the distances from nodes in the corresponding sub-group to $\vec{r}(x,y,z)$. In order to ensure the closest node to $\vec{r}(x,y,z)$ is always included in the sub-group, the size of the sub-group shall increase, thus the overall computational efficiency is reduced, as the displacement of the nodes in the QALE-FEM becomes more significant, e.g., when subjected to a uniform current. From this point of view, one needs to avoid a significant displacement of the nodes near Γ_C and the relaxation zone in order to achieve a higher robustness. As indicated above, the introduction of β in Eq. (5) brings numerical benefits. In the present hybrid model, $\beta = 0$ is assigned for nodes in the area covered by the relaxation zone of the NS solver so that the FNPT nodes in such area move primarily in vertical direction only; in other area, its value is assigned by

$$\beta = \begin{cases} 1 & d_\Gamma > D_\Gamma \\ \frac{d_\Gamma}{D_\Gamma} & d_\Gamma \le D_\Gamma \end{cases} \tag{10}$$

where D_Γ is the size of the relaxation zone of the NS solver; d_Γ is the distance from a node in the FNPT domain to the boundary of the relaxation zone. Furthermore, to ensure the accuracy of the gradient estimation using the QSFDI (so does the MLS and WLS), a sufficiently fine mesh resolution near Γ_C need to be maintain during the numerical simulation. For this purpose, a large spring stiffness are assigned to the area near Γ_C when reallocating the free surface nodes in the QALE-FEM using the spring analogy method, i.e.

$$k_{ij} = \gamma_e k_{ij}^0 \tag{11}$$

in which $k_{ij}^0$is the spring stiffness calculated using the methods presented in Ma and Yan (2009) and Yan and Ma (2010). γ_e is an additional coefficient to ensure a fine mesh resolution near Γ_C, which is given as $e^{(\hat{w}_i+\hat{w}_j)/2}$ with $\hat{w}$ being a weighting function given by $\hat{w} = 1 - \beta$. For convenience, the present hybrid model is referred to as qaleFOAM, representing the coupling between the QALE-FEM and the OpenFOAM. It is admitted that the weakly coupling using the zonal approach is not a new idea. Broadly speaking, the existing research on developing wave generation and absorbing toolkits for NS solvers (e.g., Jacobsen *et al*. (2011), Higuera *et al*. (2013), Hu *et al*. (2016)) may also be classified as a weakly coupling approach.

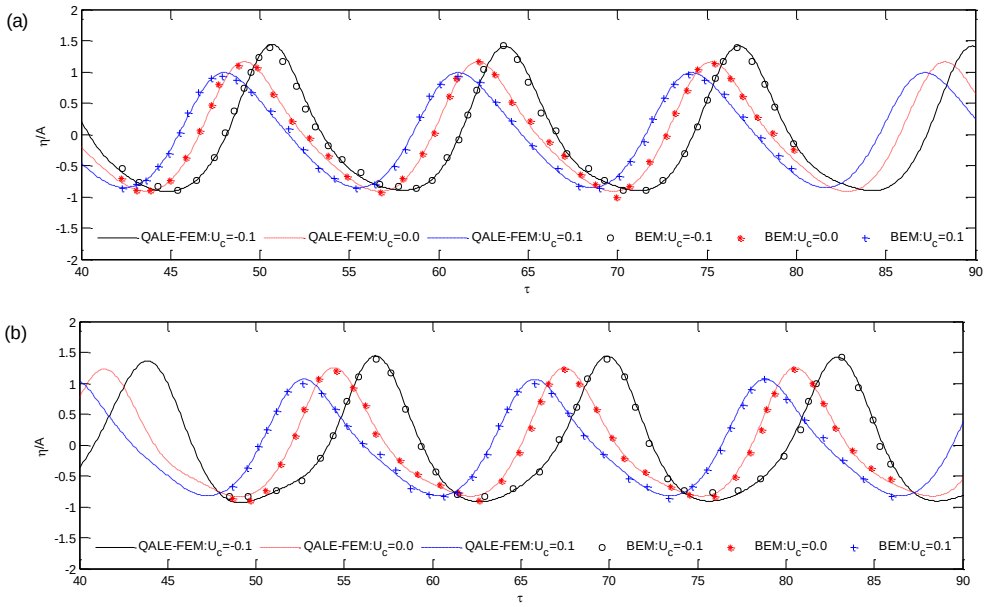

Fig. 3 Wave histories recorded at (a) x=10d from the left end and (b) x=15d from the left end in the cases with different currents (A=0.05d, ω=0.4812$\sqrt{g/d}$, $\tau = t/\sqrt{d/g}$, BEM results are duplicated from Ryu *et al*. (2003))

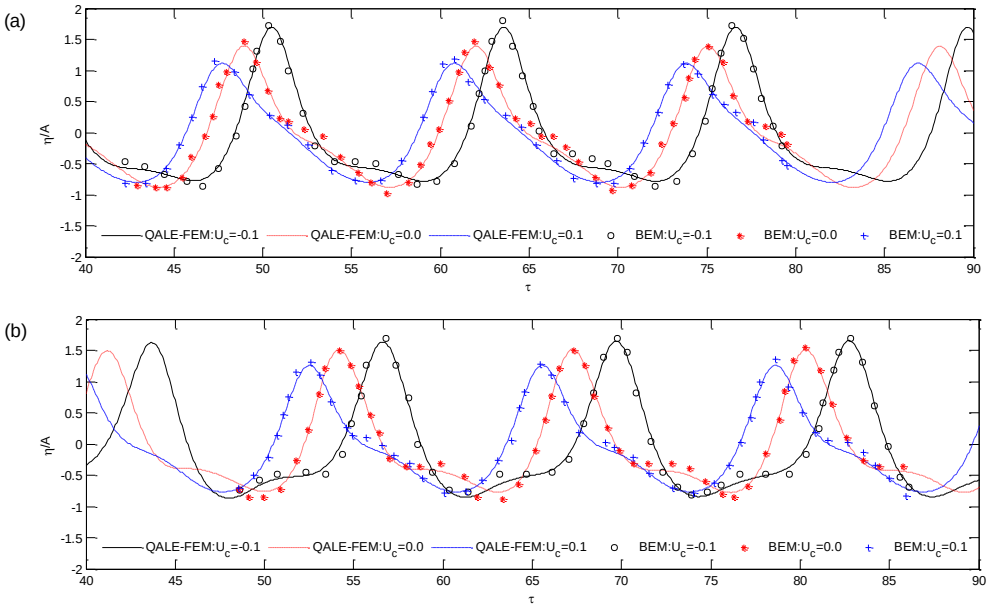

Fig. 4 Wave histories recorded at (a) x=10d from the left end and (b) x=15d from the left end in the cases with different currents (A=0.1d, ω=0.4812$\sqrt{g/d}$, $\tau = t/\sqrt{d/g}$, BEM results are duplicated from Ryu *et al*.(2003))

However, these studies are based on the use of simplified wave theories, such as linear theory, Stokes wave theories up to the fifth order, solitary wave theory, NewWave theory, which may be insufficient to deal with the problems with extreme waves. To overcome this limitation, Yan and Ma (2010) coupled the QALE-FEM with the StarCD to investigate the wind effects on freak waves, meanwhile Hildebrandt *et al*.(2013) have also coupled the FNPT model with FLUENT using a similar idea, whereas, a single interface between the FNPT and NS model is employed. Further improvement is made by introducing a relaxation zone technique to absorb the reflected waves and/or ensuring a smooth transition between the FNPT solution and the NS solutions, e.g., the recent work done by Higuera *et al*. (2018), who developed a hybrid model to combine the OpenFOAM with a Lagrangian model based on the Euler's equation using weakly coupling approach. It is noted that the OceanWave3D (Engsig-Karup *et al*. 2009) has been released within the OpenFOAM/waves2FOAM (Jacobsen *et al*. 2011). Attempts have been made to weakly coupling the OceanWave3D with the OpenFOAM for wave-structure interactions. The success of those works indicates that the weakly coupling may be sufficient, provided that the reflected waves are effectively absorbed in relaxation zone. However, to the best of the authors' knowledge, the coupling between the FNPT and two-phase NS solver using this approach for wave-structure interactions considering nonlinear effects of current has not been carried out so far. In the present qaleFOAM, the FNPT model is solved by the QALE-FEM with purposely developed techniques described above, including the ALE form of free surface boundary condition, moving-mesh algorithm for relocating the free surface nodes and a robust gradient calculation scheme, to ensure an efficient hybrid model with capacities of modelling the fully nonlinear interaction between extreme waves and a uniform current.

3. Numerical results and discussions

In this section, the qaleFOAM is validated by comparing its numerical results with those in literatures. The convergence properties and the size of the relaxation zone are also examined in order to provide a reference for future applications. The problems on uni-directional wave interacting with horizonal cylinder under the action of uniform current are focused in this section. Such problems can be considered as *y*-independent problems in the present simulation. In the simulation, the width of the numerical wave tank is taken as 4*ds*, where *ds* is the characterised mesh size on the free surface, and all parameters do not vary along *y*-direction. For convenience, the parameters used in the rest of the paper in length are nondimensionalised by the water depth *d*, time and velocity by $\sqrt{d/g}$ and $\sqrt{gd}$, respectively, force by $\rho_w g D^2 W$, where g is the gravitational acceleration, *D* and *W* are the dimeter and width of the structure, unless mentioned, otherwise.

3.1 Numerical validation of the QALE-FEM for modelling wave-current interaction

The role of the FNPT based QALE-FEM in the qaleFOAM is mainly to provide a fully nonlinear wave conditions with/without considering the uniform current. Its accuracy on modelling steep waves without current has been extensively demonstrated through comparing its predictions with experimental results and other numerical results (Yan *et al*. 2010, Ma and Yan 2009, Yan and Ma 2007, 2010, 2018, Ma *et al*. 2015, Yan *et al*. 2016). Thus, only those with current are discussed here, which include two cases considering monochromic wave, and focusing wave propagating in a uniform current. Due to the fact that no structure is involved in such cases, the origin of the coordinate system is placed at the mean position of the wavemaker at the left end of the tank.

The first case considered here is a unidirectional nonlinear monochromic wave propagating on a uniform current studied by Ryu *et al.* (2003) and Huang *et al*. (2007). To reproduce the simulations by using the qaleFOAM, the frequency (ω) of the incident wave is 0.4812, and two different wave amplitudes (*A*), i.e. 0.05 and 0.1, are used. The waves are exposed to three different current conditions, i.e., with following current (U_{cx} = 0.1), without current (U_{cx} = 0.0) and with opposing current (U_{cx} = -0.1). The simulation by the present method is carried out in a numerical tank with the length of 50. The initial mesh size on the free surface is 0.2, which is about 1/60 wavelength. The time step is chosen using the principle presented in Yan and Ma (2010). A linear wavemaker theory is used to generate the waves. Figs. 3 and 4 display the comparisons of the wave histories recorded at different positions between the results from the present method and those from the BEM by Ryu *et al.*(2003). These figures show that the agreements between the present method and the BEM (Ryu *et al*. 2003) are generally very good for different wave amplitudes and different current speeds. It implies that the improved QALE-FEM is very accurate for simulating the monochromatic waves interacting with uniform current.

The second case considered here is a focusing wave subject to uniform current, which has been experimentally investigated by Wu and Yao (2004). The focusing wave in this case is generated through a summation of a number of sine (cosine) wave components, while the displacement of the piston-type wavemaker is given by

$$S_{wm}(\tau) = \sum_{n=1}^{N} \frac{a_n}{F_n} \cos(\omega_n \tau + \varepsilon_n) \tag{12}$$

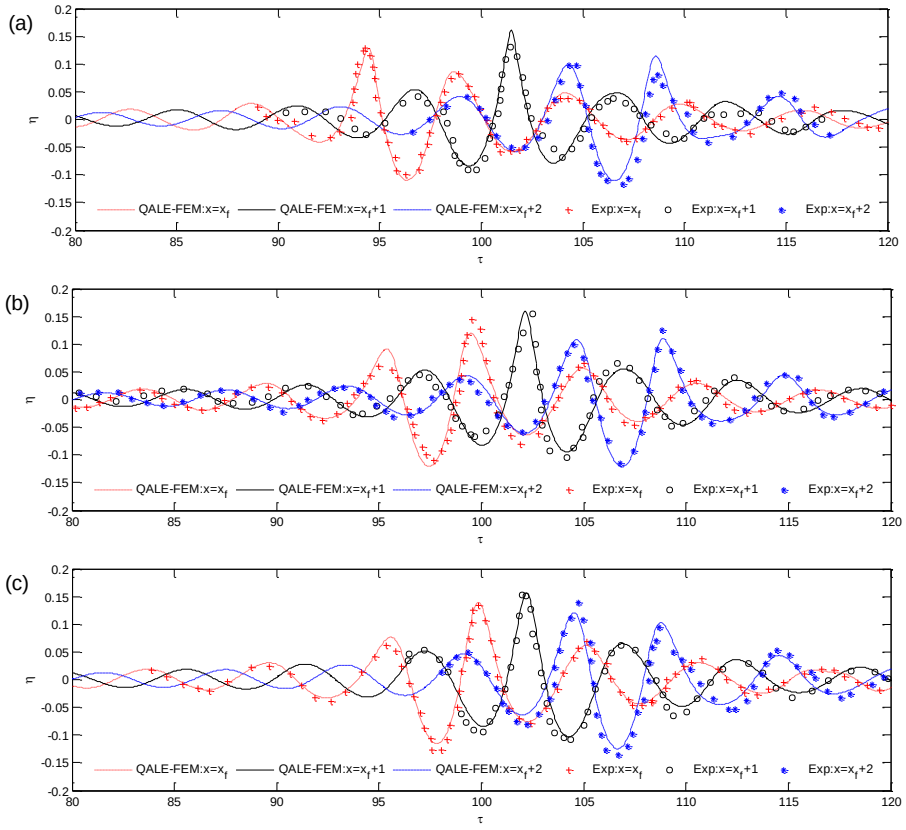

Fig. 5 Wave histories recorded at different positions in the case with (a) U_{cx}= - 0.04123$\sqrt{gd}$, (b) U_{cx}= 0 and (c) U_{cx} = 0.04123$\sqrt{gd}$ (N=32, x_f = 12.5d, τ_f = 102.5$\sqrt{d/g}$, ω_{min} = 1.0724$\sqrt{g/d}$; ω_{max} = 2.2846$\sqrt{g/d}$; $\tau = t/\sqrt{d/g}$; the experimental data from Wu and Yao (2004))

where N is the total number of components; F_n is the linear transfer function of the wavemaker for the n-th wave component; k_n and ω_n are the wave number and frequency of the n-th component, respectively. They are related to each other by the linear Doppler-shifted dispersion relation $(\omega_n - k_n U_c)^2 = k_n \tanh k_n$. For simplification, the frequency is evenly distributed in the range between the minimum (ω_{min}) and maximum frequency (ω_{max}). a_n is the amplitude of n-th component. ε_n is the phase of the n-th component and is chosen to be $k_n x_f$ - $\omega_n \tau_f$ with x_f and τ_f being the specified focusing location and time. It should be noted that the location (x_f^*) and time (τ_f^*) corresponding to the observed highest crest may be different from the expected values, x_f and τ_f, due to the nonlinearities. The input wave amplitude spectrum in this case is given by $a_n = (k_N^0 - k_n^0)/[k_n^0(k_N^0 - k_1^0)]a_1 k_1^0$, in which the superscript '0' denotes of zero current; a_1 is taken as 0.01073. The frequency ranges from 1.0724 to 2.2846. The mean group velocity (c_g) for the case without current, which is calculated using (ω_{max} - ω_{min})/(k_{max} - k_{min}), is 0.3312. The total number of wave components (N) is taken as 32. x_f and τ_f are specified as 12.5 and 102.5, respectively. The numerical simulation is carried out in a tank with length of 30, and the initial mesh size on the free surface is 0.075.

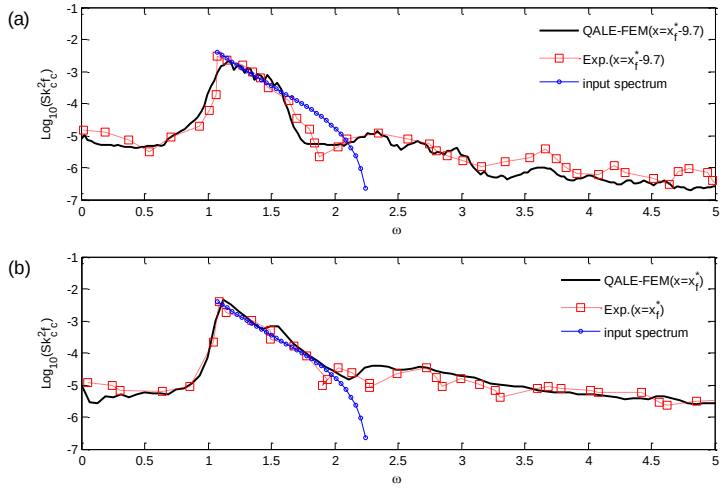

Fig. 6 Wave spectra recorded at (a) $x = x^*_f$-9.7d and (b) focusing point ($x = x^*_f$) in the case with strong opposing current (N=32, x_f = 15.0d, τ_f = 200.0$\sqrt{d/g}$, ω_{min} = 1.0724$\sqrt{g/d}$; ω_{max} = 2.2846$\sqrt{g/d}$; U_{cx}= -0.1443$\sqrt{gd}$; frequency ω in horizontal axis is non-dimensionlised by $\sqrt{g/d}$; the experimental data from Wu and Yao (2004))

Fig. 5 displays the wave histories recorded at different positions for the cases with or without current, in which it can be found that due to the presence of uniform current, the release of the wave packet on the following current was lagged, while this feature was reversed on the opposing current. Meanwhile, the numerical results agree very well with those in literature. To further demonstrate the accuracy of the QALE-FEM, comparison is also made for the wave spectrum, as shown in Fig. 6, in which qualitatively good agreement of the numerical results with the experimental data is observed. It indicates that the improved QALE-FEM successfully captured the focusing and defocusing process of the wave packet in presence of the uniform current.

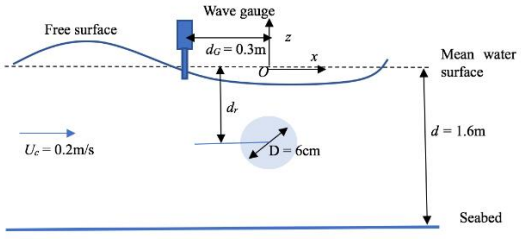

(a) Sketch of wave-current interaction with horizontal circular cylinder

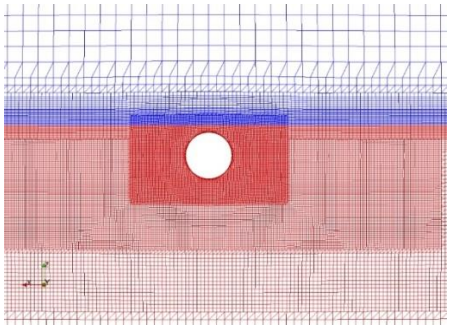

(b) Illustration of the computational mesh near the cylinder

Fig. 7 (a) Sketch of wave-current interaction with a horizontal circular cylinder (sketch is duplicated from Bai *et al.*(2017)) and (b) illustration of the computational mesh near the cylinder in the NS domain (d_r/D = 0.667, red and blue represent water and air, respectively)

Both the cases of monochromatic wave and focusing wave in presence of uniform current have well demonstrated the robustness of the improved QALE-FEM for simulating fully nonlinear wave-current interactions. Therefore, it can be effectively used to provide accurate boundary conditions for the NS domain. Next, the effectiveness of the proposed hybrid model, i.e., the qaleFOAM, will be examined.

3.2 Convergence properties of the qaleFOAM and size of relaxation zones

In this section, the qaleFOAM is applied to simulate the fully nonlinear wave-current interaction in presence of a horizontal circular cylinder, of which the configuration is described in Fig. 7(a). The problem has been experimentally and numerically investigated by Bai *et al*. (2016, 2017) in a wave flume with a mean water depth of 1.6 m. The cylinder with a nondimensional diameter D=0.0375d is placed at different locations below the mean water surface with vertical distance d_r ranging from 0 to 0.0563, yielding a ratio d_r /D within [0,1.5]. Uniform current with U_c = $0.05\sqrt{gd}$ (0.2 m/s) is imposed on regular waves with wave height of H=0.0187d. To consider different degrees of wave nonlinearities, two different wavelengths λ =12.75D and 26D are used, where the wave steepness H/λ = 0.0391 and 0.0192, respectively. A wave gauge is placed at d_G=0.1875d in front of the cylinder, meanwhile the drag and lift force on the cylinder are measured. More details about the experiments can be found in Bai *et al*. (2016, 2017). It is worth noting that in the present simulation, the length of the FNPT domain is 18.75d, slightly larger than the length of the experimental flume, i.e., 15.375d, to accommodate the numerical wave absorption in the right end of the FNPT domain, where the wave energy is dissipated in the damping zone; the length of the NS domain is 5d, the same as the length of the working section of the experimental flume, and the height of the NS domain is 1.375d. In addition, the $k-\omega$ SST model is used in the OpenFOAM/interDyMFOAM to consider the turbulence effects.

The convergence properties of the qaleFOAM depend on both of those for the QALE-FEM and the OpenFOAM. The mesh for the QALE-FEM is unstructured, as demonstrated in Fig. 2, and generated by an in-house mesh generator. It is concluded in section 3.1 that the characteristic mesh size on the free surface being approximately λ/60 and a growth factor of the mesh size from free surface to seabed (Yan and Ma 2010) being 1.7 are appropriate for achieving the convergent results by the QALE-FEM. On the other hand, the mesh used in the NS domain for the OpenFOAM/interDyMFOAM, is generated by using the snappyHexMesh, and the mesh in the area near the structure, free surface and wake behind the cylinder are refined to ensure a sufficient resolution. In order to resolve the vortex shedding from the cylinder, 5 layers of structured mesh attached to the surface of the cylinder are generated with a growth ratio of 1.3. An illustration of the mesh used in the OpenFOAM/interDyMFOAM is given in Fig. 7(b). In addition, it should be noted that a dynamic time step with Courant number of 0.25 is employed by OpenFOAM/interDyMFOAM while the time step size required by the QALE-FEM to achieve convergent result ranges from T/64 to T/200 (Yan and Ma 2010), where T is the wave period. In general, the time step size required by QALE-FEM is much larger than that by the OpenFOAM/interDyMFOAM using the Courant number control. However, the same time step sizes are used by both the QALE-FEM and the OpenFOAM/interDyMFOAM in this study. This ensures the synchronization of the simulation by using the two methodologies in time domain, which is sufficient for investigating the convergence properties of the OpenFOAM/interDyMFOAM on the mesh size. Nevertheless, one may use different time step sizes for the two methodologies with appropriate numerical interpolation to feed QALE-FEM data

to the OpenFOAM/interDyMFOAM in order to maximise the computational performance of the qaleFOAM, as utilised in Yan and Ma (2010) (Eq. (13)).

To investigate the convergence properties of the OpenFOAM/interDyMFOAM, three sets of computational mesh used in the NS domain for the case with d_r/D = 0.667 are employed, which are summarised in Table 1. While in these cases, the length of the relaxation zone D_Γ =1.5λ is employed. Waves of period T =1.733$\sqrt{d/g}$ and the corresponding wave length λ =12.75D are generated. If the mesh size being used is suitable for modelling such waves through this convergence test, it should work for the other wave condition to be simulated where it features a relatively smaller steepness. Fig. 8 compares the time histories of the drag (F_x) and the lift (F_z) force per unit width acting on the cylinder in the cases with different computational mesh. The figure shows an evident asymmetry of the drag and lift time histories about F_x =0 and F_z =0, which confirms the importance of considering the role of the nonlinearities. Meanwhile, it is observed that as the mesh size reduces, the results by using the qaleFOAM tend to be convergent. It reveals that the mesh size configuration used in case M2 is sufficient to achieve the convergent results by using the qaleFOAM, while costs less computational efforts than M3. In addition to the force, the wave elevation at different location and the wave profiles at different time are also considered as criteria in the convergent test. A similar conclusion can be made. Further convergence tests in terms of different submerge depth and wave steepness confirms the suitability of M2, while the results are omitted for the sake of the tidiness of this paper.

Another important factor influencing the robustness of the qaleFOAM is the size of the relaxation zone, D_Γ. As the increase of D_Γ, the NS domain size increases, yielding a longer CPU time to complete the simulation.

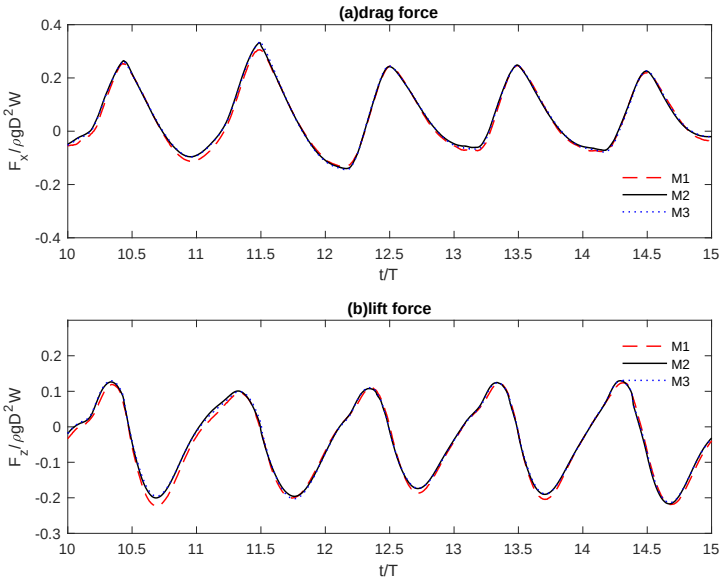

Fig. 8 Time histories of the drag (F_x) and lift (F_z) force per unit width in the cases with different mesh sizes (d_r/D = 0.667, T = 1.733$\sqrt{d/g}$, D_Γ/λ =1.5 , H/λ=0.0391, U_c = 0.05$\sqrt{gd}$)

Table 1 Summary of the computational mesh used in the NS domain for the case with d_r/D = 0.667

	Characteristic mesh size on cylinder surface (No. of grids per circumference)	Characteristic mesh size near the free surface (No. of grids per wave length)	Total number of grids
M1	0.0026 m(72)	0.0110 m (70)	52400
M2	0.0018 m(104)	0.0078 m (98)	132748
M3	0.0014 m (132)	0.0056 m (136)	334196

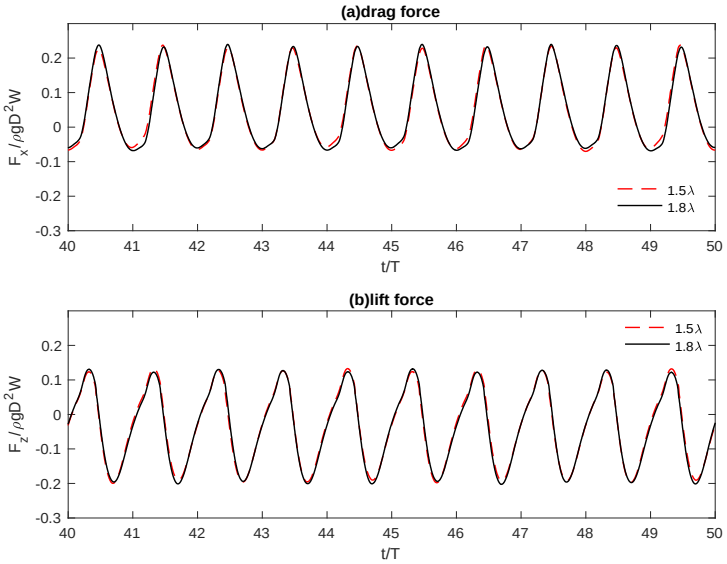

Fig. 9 Time histories of the drag (F_x) and lift (F_z) force per unit width in the cases with different sizes of the relaxation zone (d_r/D = 0.667, T = 1.733, H/λ=0.0391, U_c = 0.05, computational mesh: M2)

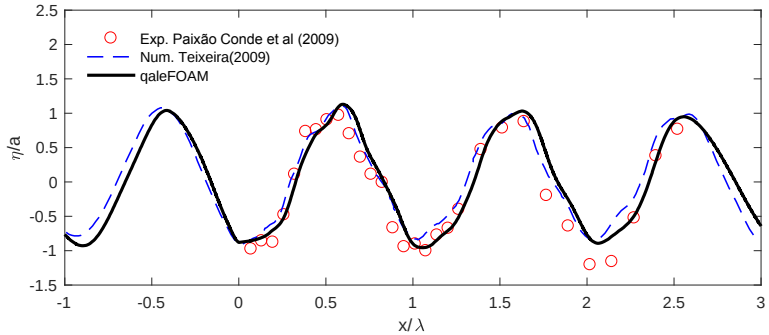

Fig. 10 Comparison of wave profile at 16.25T (a/d = 0.028, λ/d= 0.869, D/d = 0.118, d_r/D = 1.5, U_c = 0; the experimental data is duplicated from Paixão Conde *et al*. (2009) and the numerical results are duplicated from Teixeira (2009))

If the size of the relaxation zone is too small, the reflected waves due to the cylinder cannot be effectively absorbed at the boundaries Γ_C. Consequently, waves will be re-reflected from the boundaries Γ_C and modify the wave conditions near the cylinder. Such influence may be accumulated during a time-domain simulation. To examine the effectiveness of the relaxation zone technique and determine its size for achieving the best performance, a long-duration simulation is required. Therefore, a systematic numerical test by using the qaleFOAM without considering current has been carried out in order to find a suitable value of D_Γ. It is found that $D_\Gamma = 1.5\lambda$ is acceptable and no significant re-reflected waves are observed for up to 50 wave-period in the cases with different wave steepness up to wave breaking. Heuristically, the same principle should apply for the cases with uniform current. To confirm this, a corresponding case with a larger relaxation zone, i.e., 1.8λ, is carried out. Fig. 9 shows its results in comparison with the case in Fig. 8. As indicated, the drag and lift forces obtained by using a relaxation zone length $D_\Gamma = 1.5\lambda$ agree very well with those by using $D_\Gamma = 1.8\lambda$. It means that $D_\Gamma = 1.5\lambda$ is sufficient for the cases with uniform current while can maintain satisfactory computational efficiency.

3.3 Accuracy of the qaleFOAM for modelling wave-structure interaction with/without uniform current

After basic numerical tests regarding the convergence properties and the appropriate size of the relaxation zone, the qaleFOAM is firstly applied to the case without current. For such a case, the experimental studies by Paixão Conde *et al*. (2009) are used for a benchmark test. This case has been numerically investigated by various numerical codes, including the FNPT solved by using BEM (Paixão Conde *et al*. 2009) and the QALE-FEM (Yan *et al*. 2010), a NS solver by Teixeira (2009). In this case, the cylinder placed in a wave flume with mean water depth of 0.425 m. The diameter (D) of the cylinder is $0.118d$. The submerged depth of the cylinder is $1.5D$ and the distance from the wavemaker to its centre is $14.706d$. The length of the FNPT domain of the qaleFOAM is the same as the experiments, i.e., $47d$. The length and the height of the NS domain are $11.65d$ and $1.47d$, respectively, in which $D_\Gamma = 1.5\lambda$ is applied. The wave amplitude is $0.028d$ and the wavelength is $1.869d$. Fig. 10 compares the wave profiles at the instant of $16.25T$. For the purpose of comparison, the experimental data by Paixão Conde *et al*. (2009) and the numerical results by Teixeira (2009) are also plotted together. A satisfactory agreement between the present numerical results and others has been observed, which indicates that the present hybrid model qaleFOAM successfully captured the surface spatial distribution at the specified time instant.

The wave-structure interaction with presence of uniform current is then considered. For validation purpose, the experiments run by Bai *et al*. (2017), which is briefed in the beginning of Section 3.2, are used. The wave elevation recorded at the wave gauge located at 0.3 m ($0.1875d$) in front of the cylinder, the drag and lift forces acting on the cylinder are predicted by the present qaleFOAM and compared with the corresponding experimental data and numerical results by Bai *et al*. (2017), who applied a NS solver FLUENT for the numerical practices, where the RANS equations are solved by the finite volume method, and the Reynolds stress term is modeled by the RNG $k-\varepsilon$ turbulence model. The pressure-velocity coupling is evaluated by using the SIMPLE (Semi-Implicit Method for Pressure Linked Equations) algorithm. Two-phase flow is considered and the volume of fluid (VOF) method is used to track the free water surface. In the numerical tank used by Bai *et al*. (2017), inlet and outlet conditions with constant velocity of 0.2 m/s are applied at two ends of the numerical wave tank; the wave is generated by a wavemaker with a dynamic mesh technique to deal with the motion of the mesh conforming to wavemaker motion.

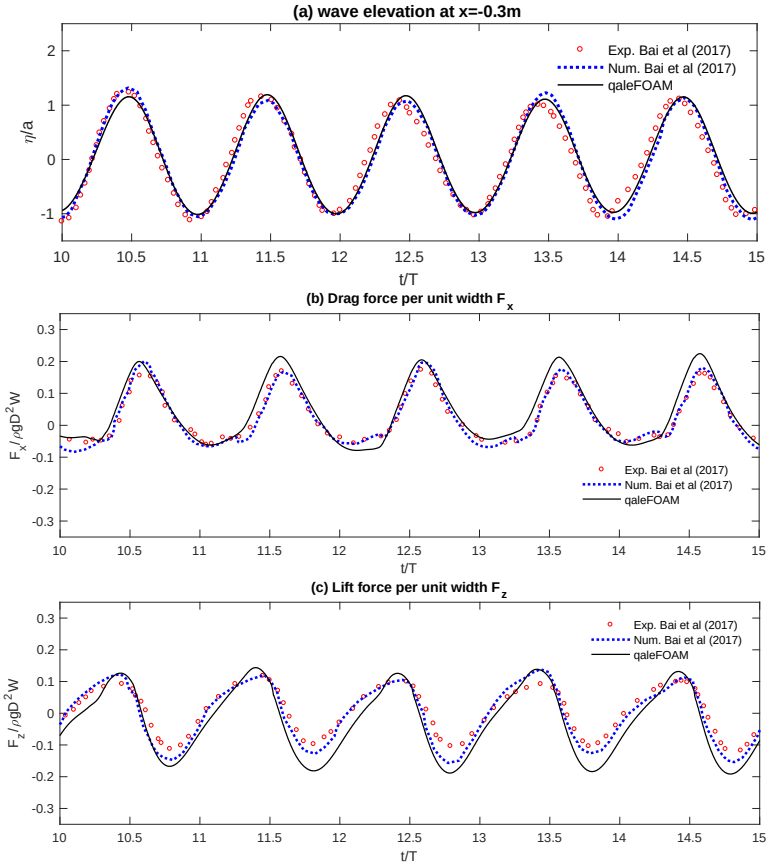

Fig. 11 Time histories of (a) wave elevation recorded at x = -0.3 m (0.1875d front of the centre of the cylinder), (b) drag force per unit width (F_x) and (c) lift force per unit width (F_z) in the case with fully submerged cylinder (d_r/D = 0.667, $T = 1.733\sqrt{d/g}$, D_Γ =1.5λ , $U_c = 0.05\sqrt{gd}$, the time in the qaleFOAM is shifted to match the phase, numerical and experimental results are duplicated from Bai *et al*. (2017))

The qaleFOAM simulation starts from the rest, i.e., the wave elevation and the velocity of the fluid being zero in the beginning. The wavemaker in the qaleFOAM is a piston wavemaker and is installed at the left end of the tank. Such configurations may be considerably different from the experimental and numerical configurations by Bai *et al*. (2017) due to a lack of information regarding the initial conditions and the shape/location of the wavemaker. Consequently, both the wave elevation and the force acting on the cylinder in the transient stage of the qaleFOAM simulation are different from those presented in Bai *et al*. (2017). However, one may agree that the corresponding results at the steady stage of the qaleFOAM simulation, i.e. after 20 wave periods, are comparable with the experimental and/or numerical results in the late stage, e.g., those in the last 5 periods, available in Bai *et al*. (2017). For this purpose, the results of the qaleFOAM are shifted in the time frame for comparison. Some comparisons are shown in Figs. 11 and 12 for the cases with d_r/D = 0.667 and d_r/D = 0, respectively. Once again, acceptable agreements between the results by the present qaleFOAM and the experimental/numerical results in Bai *et al*. (2017) are observed.

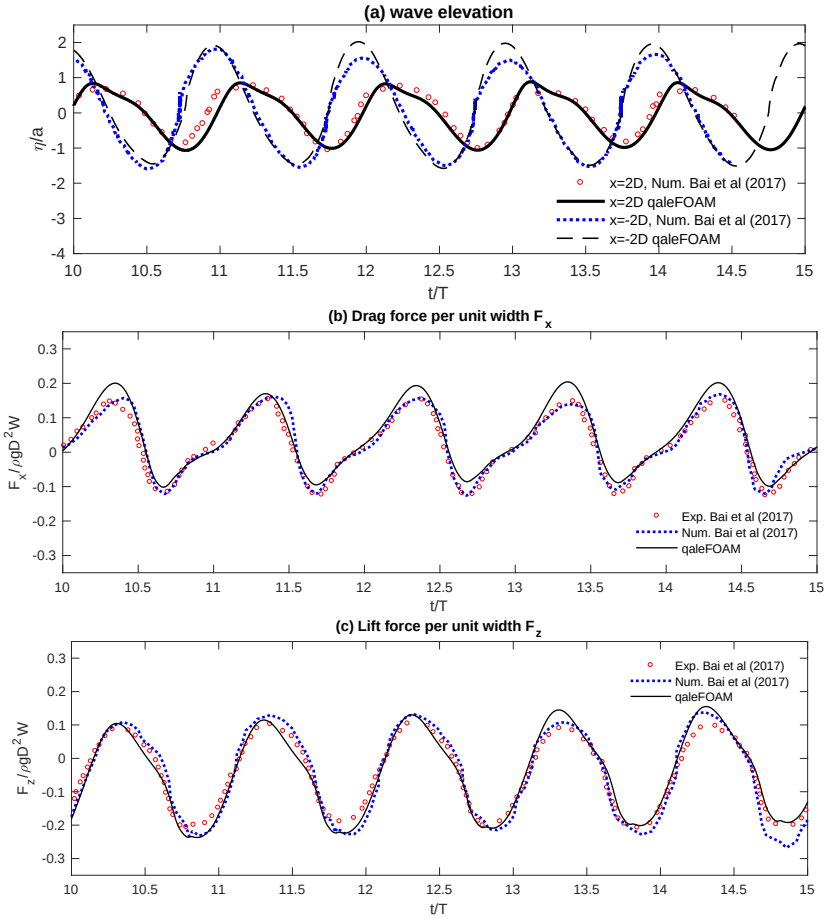

Fig. 12 Time histories of (a) wave elevation recorded at $x = \pm 2D$, (b) drag force per unit width (F_x) and (c) lift force per unit width (F_z) in the case with partially submerged cylinder (d_r/D = 0, $T = 1.733\sqrt{d/g}$, $D_\Gamma = 1.5\lambda$, $U_c = 0.05\sqrt{gd}$, the time in the qaleFOAM is shifted to match the phase, numerical and experimental results are duplicated from Bai *et al*. (2017))

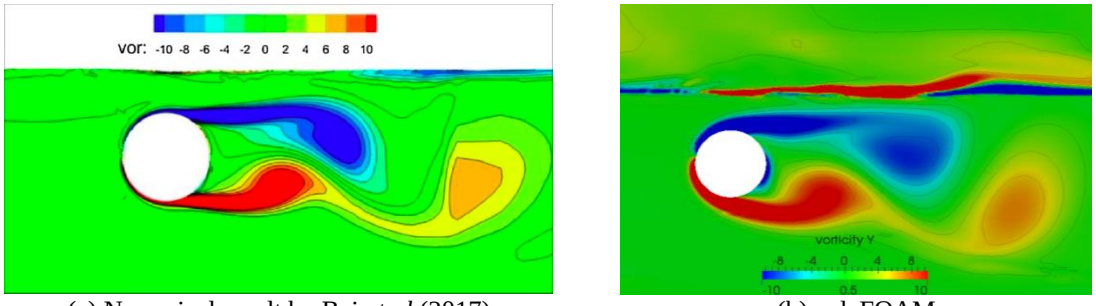

(a) Numerical result by Bai *et al*.(2017) (b) qaleFOAM

Fig. 13 Comparison of the vorticity distribution near the structure (d_r/D = 1.0, $D_\Gamma = 1.5\lambda$, $U_c = 0.05\sqrt{gd}$, no incident waves; (a) is duplicated from Fig. 14 of Bai *et al*. (2017))

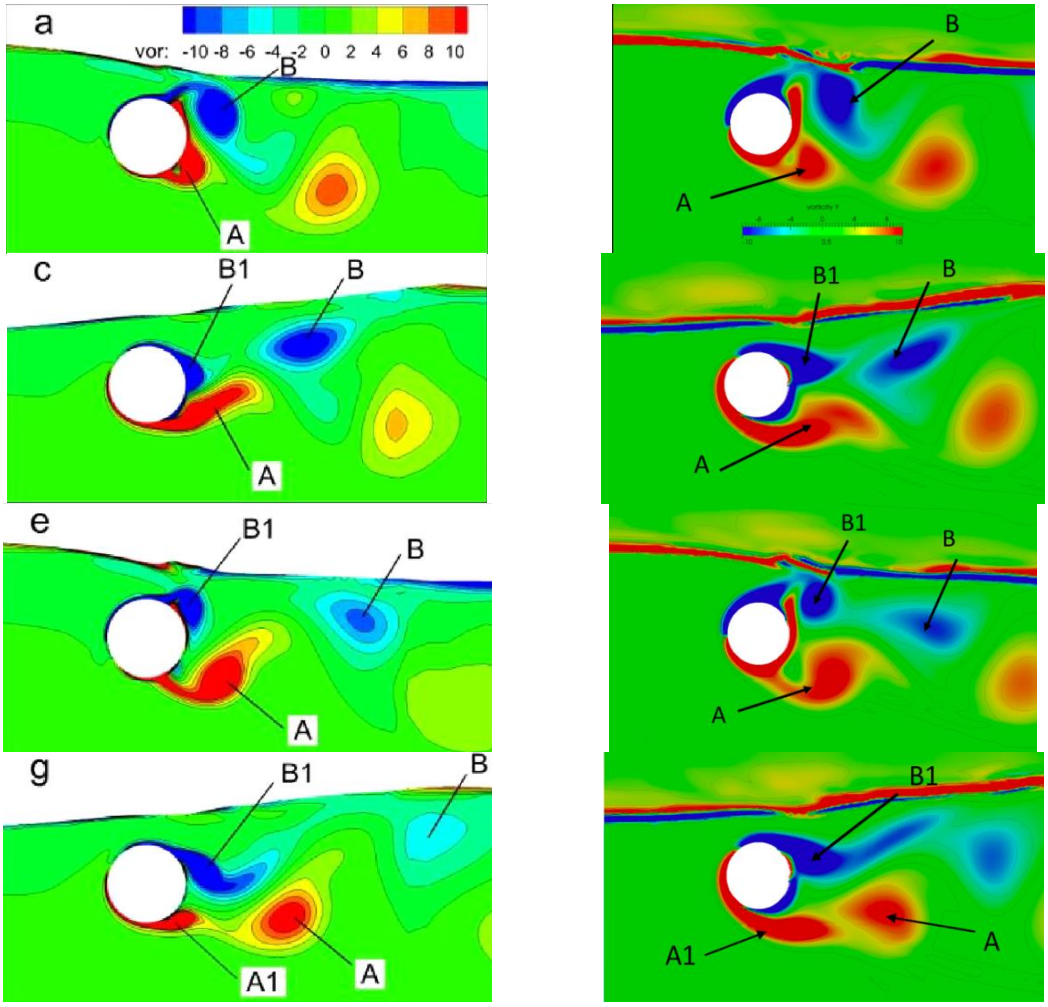

Fig. 14 Comparison of the vorticity distribution near the structure at different time instants (d_r/D = 1.0, T = 1.733$\sqrt{d/g}$, D_Γ =1.5λ , U_c = 0.05$\sqrt{gd}$, left column is the numerical results duplicated from Bai *et al*. (2017); right column is the numerical results obtained by using the qaleFOAM)

It shall be noted that the force presented in Figs. 11 and Fig. 12 are obtained by integrating the pressure and viscous stress on the surface of the cylinder. In addition to the viscous effects, the qaleFOAM takes the advantages of the NS solver on its capacity of modelling small-scale turbulence, e.g. the vortex shedding, and overcomes the limitation of the FNPT model (e.g., Yan *et al*. 2010) on modelling rotational flow. This is demonstrated by Figs. 13 and 14, which compares the vorticity distribution near the cylinders between the results by the qaleFOAM and the corresponding results by Bai *et al*. (2017). For the case without incident waves (Fig. 13), the present results by the qaleFOAM, where $k-\omega$ SST is employed for turbulence modelling, agree well with the numerical results by Bai *et al*. (2017), who used RNG $k-\varepsilon$ model for turbulence modelling. For the case with incident waves (Fig. 14), Bai *et al*. (2017) gave the vorticity distribution within two wave periods but did not specify the exact time for the instants. Similar to

the results shown in Figs. 11 and 12, the vorticity distribution shown in the right column of Fig. 14 are at the steady state of the qaleFOAM simulation, i.e., after 20 wave periods, ensuring the free surface profile at Fig. 14(a) obtained from the qaleFOAM (right figure) matching that from Bai *et al*. (2017) (left figure). As observed from Fig. 14, despite different turbulent models are used, the typical feature of the vorticity distributions at different instants predicted by the qaleFOAM primarily agrees with the numerical results by Bai *et al*. (2017), except the vortex attached to the upper surface of the cylinder (near the free surface).

Furthermore, the qaleFOAM takes the advantages of the FNPT modelling on its high computational efficiency for modelling the extreme wave generation, evolution and propagation in a large space.

In the cases with wave and current presented in this paper, the length of the NS (5d) is approximately 1/3.75 of the length of the overall computational domain. The simulation is parallelly run using OpenMPI in a workstation equipped with Intel Xeon E5-2660 v3(2.6GHz). The total elapsed time with 8-core in parallel computation to achieve the results up to 50 wave periods, e.g., those presented in Fig. 9, using the computational grid M2 is approximately 12 hours. At each time step, the CPU time spent by the FNPT is about 8%, which is negligible compared with those spent by the NS solver. One may envisage that if a NS solver (e.g. the OpenFOAM/interDyMFOAM) covering the entire computational domain, the CPU time to achieve the same results shown in Fig. 9 may be approximately 4 times of the CPU time spent by the qaleFOAM, providing a similar mesh resolution can be used in the entire computational domain. Clearly, as the percentage of the NS domain in the entire computational domain reduces, the improvement of the efficiency of the qaleFOAM over the NS solvers become more significant.

4. Conclusions

This paper presents a zonal hybrid model, qaleFOAM, combining the QALE-FEM based on the FNPT and the OpenFOAM/interDyMFOAM, which solves two-phase incompressible NS model using FVM and VOF. The qaleFOAM takes the advantages of the multiple NS solver on its capacity of modelling breaking wave impacts and viscous/turbulent impact in the small area of interest, e.g., near the structure surface, and that of the FNPT model on higher computational efficiency for modelling the extreme wave generation, evolution and propagation in a large space. A weakly coupling approach is implemented in this paper. In order to maximise the computational efficiency and capacity, further developments have been made in the QALE-FEM. These include (1) derivation of an ALE form of the free surface boundary conditions to tackle the challenges in modelling the wave-current interaction; and (2) application of the QSFDI for estimating the velocity on the boundary of the NS domain and in the relaxation zone. Unlike our previous works, e.g., the hybrid model coupling the QALE-FEM with the StarCD (Yan and Ma 2010), a relaxation zone is introduced near the coupling boundary for absorbing the reflected waves and/or ensuring a smooth transition between the FNPT solution and the NS solutions. Compared with other existing hybrid models using the same strategy but solving the FNPT using other methods, e.g., the OceanWave3D toolkit or BEM, the capacity and the computational efficiency of the QALE-FEM may make the qaleFOAM be more suitable to deal with highly nonlinear wave interaction with structures with/without action of uniform current.

Numerical investigations on wave-structure interaction with/without current are carried out to quantify the size of the relaxation zone and to assess the convergence and accuracy of the

qaleFOAM. It is concluded that

- The accuracy of the QALE-FEM with further developments is satisfactory for modelling the fully nonlinear interaction between the extreme waves and uniform current, yielding a well-predicted flow condition for the OpenFOAM simulation in the NS domain.
- The size of the relaxation zone may be a minimum of 1.5 characterised wave length for the cases shown in this paper.
- The convergent solutions of the qaleFOAM agree with the experimental data and other numerical results available in the literatures.

It is admitted that choosing the $k-\omega$ SST in the applications is based on our numerical tests without considering free surface flow. Although sufficient work has been done to ensure the convergence of the present model, the suitability of the turbulence modelling, as well as the configuration of the wall function, in the cases with free surface waves, in particular when the structure is located close to the free surface, may need to be further investigated. Nevertheless, it shall not comprise the main contribution of this paper on developing the hybrid model. Although only *y*-independent problems with a fixed structure are focused in this paper, in which a fixed Eulerian mesh is used in the NS domain, there is no theoretical restriction for the qaleFOAM to be applied to 3D problems with structures in motions (wave excited motion or forward speeding). The outcome will be presented elsewhere. It is also worth noting that the QALE-FEM has been successfully coupled with a single-phase NS solver, MLPG-R (Yan and Ma 2017), using two-way (strong) zonal coupling strategy. This will be extended to the qaleFOAM in the near future.

Acknowledgments

The authors gratefully acknowledge the financial support of EPSRC projects (EP/L01467X/1, EP/N006569/1 and EP/N008863/1).

References

Bai, J., Ma, N. and Gu, X. (2016), "Numerical study of the interaction between combined wave-current and a horizontal cylinder close to the free surface", *Proceedings of the 26th International Ocean and Polar Engineering Conference*, Rhodes, Greece.

Bai, J., Ma, N. and Gu, X. (2017), "Study of interaction between wave-current and the horizontal cylinder located near the free surface", *Appl. Ocean Res.*, **67**, 44-58

Biausser, B., Fraunie, P., Grilli, S.T. and Marcer, R. (2004), "Numerical analysis of the internal kinematics and dynamics of 3-D breaking waves on slopes", *Int. J. Offshore Polar Eng.*, **14**, 247-256.

Büchmann, B., Ferrant, P. and Skourup, J. (2000), "Run-up on a body in waves and current. Fully Nonlinear and finite-order calculations", *Appl. Ocean Res.*, **22**, 349-360.

Celebi, M.S. (2001), "Nonlinear transient wave-body interactions in steady uniform current", *Comput. Method. Appl. Mech.Eng.*, **190**, 5149-5172.

Chaplin, J.R. and Subbiah, K. (1997), "Large scale horizontal cylinder forces in waves and currents", *Appl. Ocean Res.*, **19**, 211-223.

Chen, W., Panchang, V. and Demirbilek, Z. (2005), "On the modelling of wave-current interaction using the elliptic mid-slope wave equation", *Ocean Eng.*, **32**, 2135-2164.

Chung, M.H. (2016), "Two-degree-of-freedom vortex induced vibration of low-mass horizontal circular cylinder near a free surface at low Reynolds number", *Int. J. Heat Fluid Fl.*, **57**, 58-78.

Colicchio, G., Greco, M. and Faltinsen, O.M. (2006), "A BEM-Level set domain decomposition strategy for non-linear and fragmented interfacial flows", *Int. J. Numer. Meth. Eng.*, **67**, 1385-1419.

Dommermuth, D. and Yue, D.K.P. (1987), "A high-order spectral method for the study of nonlinear gravity waves", *J. Fluid Mech.*, **184**, 267-288.

Edmund, D.O., Maki, K.J. and Beck, R.F. (2013), "A velocity-decomposition formulation for the incompressible Navier-Stokes equations", *Comput. Mech.*, **52**, 669-680.

Engsig-Karup, A.P., Bingham, H.B. and Lindberg, O. (2009), "An efficient flexible-order model for 3D nonlinear water waves", *J. Comput. Phys.*, **228**, 2100-2118.

Feng, A. and Bai, W. (2016), "Numerical simulation of wave radiation and diffraction problems with current effect", *Proceedings of the 12th Pacific-Asia Offshore Mechanics Symposium*, Gold Coast, Australia.

Ferrant, P. (1997), "Nonlinear wave-current interactions in the vicinity of a vertical cylinder", *Proceeding of 12th International Workshop on Waves and Floating Bodies*, Marseille, France.

Ferrant, P. (2001), "Runup on a cylinder due to waves and current: Potential flow solution with fully nonlinear boundary conditions", *Int. J. Offshore Polar Eng.*, **11**, 33-41.

Ferrant, P., Gentaz, L., Alessandrini, B. and Le Touze, D. (2003), "A potential/RANSE approach for regular water wave diffraction about 2D structures", *Ship Technol. Res.*, **50**, 165-171.

Ferrant, P., Gentaz, L., Monroy, C., Luquet, R., Ducrozet, G., Alessandrini, B., Jacquin, E. and Drouet. A. (2008), "Recent advances towards the viscous flow simulation of ships manoeuvring in waves", *Proceeding of the 23rd International Workshop on Water Waves and Floating Bodies*, Jeju, Korea.

Fourtakas, G., Stansby, P.K., Rogers, B.D., Lind, S. J., Yan, S. and Ma, Q.W. (2017), "On the coupling of Incompressible SPH with a Finite Element potential flow solver for nonlinear free surface flows", *Proceedings of the 27th International Offshore and Polar Engineering Conference*, San Francisco, USA.

Fujima, K., Masamura, K. and Goto, C. (2002), "Development of the 2D/3D hybrid model for tsunami numerical simulation", *Coast. Eng. J.*, **44**, 373–397.

Grue, J. and Jensen, A. (2012), "Orbital velocity and breaking in steep random gravity waves", *J. Geophys. Res.*, **117**, 1-16.

Guo, L., Sun, D.P. and Wu, H. (2012), "A new numerical wave flume combining the 0–1 type BEM and the VOF method", *J. Hydrodynam., Ser. B*, **24**, 506–517.

Higuera, P., Buldakov, E. and Stagonas, D. (2018), "Numerical modelling of wave interaction with an FPSO using a combination of OpenFOAM and Lagrangian models", *Proceedings of the 28th International Offshore and Polar Engineering Conference*, Sapporo, Japan.

Higuera, P., Lara, J.L. and Losada, I.J. (2013), "Realistic wave generation and active wave absorption for Navier-Stokes models", *Coast.Eng.*, **71**, 102-118.

Hildebrandt, A., Sriram, V. and Schlurmann, T. (2013), "Simulation of Focusing Waves and Local Line Forces due to Wave Impacts on a Tripod Structure", *Proceedings of the 23rd International Offshore and Polar Engineering Conference*, Anchorage, Alaska.

Hu, K., Fu, S., Ma, L. and Song, L. (2016), "Nonlinear hydrodynamics of a floating cylinder in oscillatory flow alone and combined with a current", *J. Waterw, Port, C. Ocean Eng.*, **143**(2), 04016015

Hu, Z.Z., Greaves, D. and Raby, A. (2016), "Numerical Wave Tank Study of Extreme Waves and Wave-Structure Interaction Using OpenFoam®", *Ocean Eng.*, **126**, 329-342.

Huang, C., Tang, H. and Wang, C. (2007), "A 2D fully nonlinear wave-current numerical wave tank based on BEM", *Proceeding of the 17th International Offshore and Polar Engineering Conference*, Lisbon, Portugal.

Isaacson, M. and Cheung, K.F. (1993), "Time-domain solution for wave-current interactions with a two-dimensional body", *Appl. Ocean Res.*, **15** 39-52.

Jacobsen, N.G., Fuhrman, D.R. and Fredsøe, J. (2011), "A wave generation toolbox for the opensource CFD library: OpenFoam", *Int. J. Numer.Meth. Fl.*, **70**, 1073-1088.

Janssen, C.F., Grilli, S.T. and Krafczyk, M. (2010), "Modeling of wave breaking and wave-structure interactions by coupling of fully nonlinear potential flow and lattice-boltzmann models", *Proceedings of the 20th Offshore and Polar Engineering Conference*, Beijing, China.

Kharif, C., Pelinovsky, E. and Slunyaev, A. (2009), "Rogue waves in the ocean", Springer-Verlag Berlin Heidelberg.

Kim, D. and Kim, M. (1997), "Wave-current-body interaction by a tune-domain high-order boundary element method", *Proceedings of the 7th International Offshore and Polar Engineering Conference*, Honolulu, Hawaii, USA.

Kim, M.H., Celebi, M.S. and Kim, D.J. (1998), "Fully nonlinear interactions of waves with a three-dimensional body in uniform currents", *Appl. Ocean Res.*, **20**, 309-321.

Kim, S.H., Yamashiro, M. and Yoshida, A. (2010), "A simple two-way coupling method of BEM and VOF model for random wave calculations", *Coast. Eng.*, **57**, 1018-1028.

Kim, S.Y., Kim, K.M., Park, J.C., Jeon, G.M. and Chun, H.H. (2016), "Numerical simulation of wave and current interaction with a fixed offshore substructure", *Int. J. Naval Architect.Ocean Eng.*, **8**, 188-197.

Lachaume, C., Biausser, B., Grilli, S.T., Fraunie, P. and Guignard, S. (2003), "Modeling of breaking and post-breaking waves on slopes by coupling of BEM and VOF methods", *Proceeding of the 13th International Offshore Polar Engineering Conference*, Honolulu, USA.

Lavrenov, I.V., Porubov, A.V. (2006), "Three reasons for freak wave generation in the non-uniform current", *Eur. J. Mech. B Fluid*, **25**, 574-585.

Li, Y. and Lin, M., (2010), "Hydrodynamic coefficients induced by waves and currents for submerged circular cylinder", *Procedia Eng.*, **4**, 253-261.

Liang, H., Zong, Z., Zou, L., Zhou, L. and Sun, L. (2014), "Vortex shedding from a two-dimensional cylinder beneath a rigid wall and a free surface according to the discrete vortex method", *Eur. J. Mech. B/Fluid*, **43**, 110-119.

Lin, P. and Li, C.W. (2003), "Wave-current interaction with a vertical square cylinder", *Ocean Eng.*, **30**, 855-876.

Luquet, R., Ducrozet, G., Gentaz, L., Ferrant, P. and Alessandrini, B. (2007), "Applications of the SWENSE Method to seakeeping simulations in irregular waves", *Proceedings of the 9th Int. Conf. on Num. Ship Hydro*., Ann Arbor, Michigan,

Ma, Q.W. and Yan, S. (2009), "QALE-FEM for numerical modelling of nonlinear interaction between 3D moored floating bodies and steep waves", *Int. J. Numer. Method. Eng.*, **78**, 713-756.

Ma, Q.W., Yan, S., Greaves, D., Mai, T. and Raby, A. (2015), "Numerical and experimental studies of Interaction between FPSO and focusing waves", *Proceedings of the 25th International Ocean and Polar Engineering Conference*, Kona, Hawaii, USA.

Narayanaswamy, M., Crespo, A.J.C., Gomez-Gesteira, M. and Dalrymple, R.A. (2010), "SPHyiscs-FUNWAVE hybrid model for coastal wave propagation", *J. Hydraul. Res.*, **48**, 85-93.

Ning, D., Lin, H., Teng, B. and Zou, Q. (2014), "Higher harmonics induced by waves propagating over a submerged obstacle in the presence of uniform current", *China Ocean Eng.*, **28**, 725-738

Ozdil, N.F.T. and Akilli, H. (2015), "Investigation of flow structure around a horizontal cylinder at different elevations in shallow water", *Ocean Eng.*, **96**, 56-67.

Paixão Conde, J.M., Didier, E., Lopes, M.F.P. and Gato, L.M.C. (2009), "Nonlinear wave diffraction by submerged horizontal circular cylinder", *Int. J. Offshore Polar Eng.*, **19**,198-205.

Reichl, P., Hourigan, K. and Thompson, M.C. (2005), "Flow past a cylinder close to a free surface", *J. Fluid Mech.*, **533**, 269-296.

Rusche, H. (2002), "Computational fluid dynamics of dispersed two-phase flows at high phase fractions", PhD thesis, Imperial College, London.

Ryu, S., Kim, M.H. and Lynett, P.J. (2003), "Fully Nonlinear wave-current interactions and kinematics by a BEM-based numerical wave tank", *Comput. Mech.*, **32**, 336-346.

Sriram, V., Ma, Q.W. and Schlurmann, T. (2014), "A hybrid method for modelling two dimensional non-breaking and breaking waves", *J. Comput. Phys.*, **272**, 429-454.

Stringer, R.M., Zang, J. and Hillis, A.J. (2014), "Unsteady RANS computations of flow around a circular cylinder for a wide range of Reynolds numbers", *Ocean Eng.*, **87**, 1-9.

Teixeira, T.R.F. (2009), "Numerical simulation of the interaction of a regular wave and a submerged cylinder", *Therm. Eng.*, **8**, 78-83

Teng, B., Zhao, M. and Bai, W. (2001), "Wave diffraction in a current over a local shoal", *Coast. Eng.*, **42**, 163-172.

Wang, J., Ma, Q.W. and Yan, S. (2016), "A hybrid model for simulating rogue waves in random seas on a large temporal and spatial scale". *J. Comput. Phys.*, **313**, 279-309.

Wang, J., Ma, Q.W. and Yan, S. (2018), "A fully nonlinear numerical method for modelling wave-current interactions", *J. Comput. Phys.*, **369**, 173-190.

Wu, C.H. and Yao, A. (2004), "Laboratory measurements of limiting freak waves on current", *J. Geophys. Res.*, **109**, C12002, dio:10.1029/2004JC002612.

Xiao, H., Huang, W., Tao, J. and Liu, C. (2013), "Numerical modelling of wave-current forces acting on horizontal cylinder of marine structures by VOF method", *Ocean Eng.*, **67**, 58-67.

Yan, S. and Ma, Q.W. (2007), "Numerical simulation of fully non-linear interaction between steep waves and 2D floating bodies using the QALE-FEM method", *J. Comput. Phys.*, **221**, 666-692.

Yan, S. and Ma, Q.W. (2010), "QALE-FEM for modelling 3D overturning waves", *Int. J. Numer. Meth. Fl.*, **63**, 743-768

Yan, S. and Ma, Q.W. (2010), "Numerical simulation of interaction between wind and 2D freak waves", *Eur. J. Mech.B/Fluids*, **29**, 18-31.

Yan, S. and Ma, Q.W. (2017), "A hybrid approach coupling MLPG-R with QALE-FEM for modelling fully nonlinear water waves", *Proceedings of the 27th International Offshore and Polar Engineering Conference*, San Francisco, USA.

Yan, S., Ma, Q.W. and Adcock, T. (2010), "Investigations of freak waves on uniform current", *Proceeding of the 25th International Workshop on Water Waves and Floating Bodies*, Harbin, China.

Yan, S., Ma, Q.W. and Wang, J. (2018), "Quadric SFDI for Laplacian Discretization in Lagrangian Meshless Methods", CMES - Computer Modeling in Engineering and Sciences, (submitted).

Yan, S., Ma, Q.W., D'Mello, C. and Zhang, L. (2010), "Numerical investigation of fully nonlinear interaction between freak waves and 2D submerged cylinder", *Proceeding of the 20th International Offshore Polar Engineering Conference*, Beijing, China.

Yan, S., Ma, Q.W., Wang, J. and Zhou, J. (2016), "Self-adaptive wave absorbing technique for nonlinear shallow water waves", *Proceeding of the ASME 35th International Conference on Ocean, Offshore and Arctic Engineering*, Busan, South Korea.

KA